Miscibility in systems containing (poly(oxymethylene) ethers (OME) + hydrocarbons + water)

Christian F. Breitkreuz[a], *Alexander Holzer*[b], *Thorsten Fuchs*[b], *Michael Günthner*[b], *Hans Hasse*[a,]*

[a] Laboratory of Engineering Thermodynamics (LTD), Technische Universität Kaiserslautern (TUK), Erwin-Schrödinger-Str. 44, 67663 Kaiserslautern, Germany

[b] Institute of Vehicle Propulsion Systems (LAF), Technische Universität Kaiserslautern (TUK), Erwin-Schrödinger-Str. 44, 67663 Kaiserslautern, Germany

*Corresponding author, Email address: hans.hasse@mv.uni-kl.de

Keywords: liquid-liquid equilibrium, miscibility, dodecane, hexadecane, toluene, water, HVO, hydrogenated vegetable oil, OME, poly(oxymethylene) dimethyl ether

COSMO-RS	Conductor like screening model for real solvents
C12	n-dodecane
C16	n-hexadecane
EOS	Equation of state

Abstract

Poly(oxymethylene) dimethyl ethers (OME) are interesting synthetic fuels: they have better combustion properties than fossil diesel fuel and can be obtained from renewable resources. Furthermore, they can be blended with hydrogenated vegetable oils (HVO) to obtain a new class of environmentally benign fuels. However, it has been observed in technical processes that initially homogeneous mixtures of (OME + HVO) split into two liquid phases after some time, which is unacceptable for use as fuels. It is assumed that this de-mixing is a consequence of the uptake of small amounts of water from the air by the mixtures. However, up to now, only qualitative information on this phenomenon was available. We have, therefore, carried out systematic experimental studies of liquid-liquid equilibria (LLE) and liquid-liquid-liquid equilibria (LLLE) in ternary model systems of the type (OME + n-alkane + water) at temperatures between 265 to 293 K. The n-alkanes were (n-dodecane, n-hexadecane); two different OME were studied, OME_2

HVO	Hydrogenated vegetable oils
LLE	Liquid-liquid equilibria
LLLE	Liquid-liquid-liquid equilibria
NMR	Nuclear magnetic resonance
OME	Poly(oxymethylene) dimethyl ethers
PC-SAFT	Perturbated chain statistical associating fluid theory
UNIFAC	Universal quasichemical functional group activity coefficients
Tol	Toluene
W	Water

and OME_4, respectively. Additionally, also multicomponent mixtures containing different OME and mixtures containing additionally the aromatic hydrocarbon toluene were studied. The results were modeled using UNIFAC, a group-contribution model of the Gibbs excess energy, and a good correlation of the observed complex phase behavior was obtained. The results from the present work confirm that the uptake of small amounts of water is the reason for the phase split observed in technical (OME + HVO) mixtures. Measures to circumvent this problem are discussed.

1. Introduction

The use of synthetic fuels produced from renewable resources can make a significant contribution to moving away from fossil fuels and, thus, reducing greenhouse gas emissions. [1–4] Furthermore, synthetic fuels can offer also additional advantages such as lower emissions of soot or nitrous oxides.[3,5] Two particularly interesting synthetic fuels are poly(oxymethylene) dimethyl ethers (OME) and hydrogenated vegetable oils (HVO).

OME are oligomers with the general structure CH_3-O-$(CH_2O)_n$-CH_3 with $n \geq 2$. We use OME here to designate OME in general and OME_n to designate a specific OME. For the use as fuels OME_n with $3 \leq n \leq 5$ are most interesting. [4,6,7] These oligomers have similar physical properties as fossil diesel but produce much less soot upon combustion because they contain oxygen in their backbone. OME are produced from methanol, which, in turn, is produced from synthesis gas, which can be obtained from biogas as well as from carbon dioxide and hydrogen, i.e. OME can be obtained from renewable resources. [8,9] This enables establishing a closed carbon cycle to minimize greenhouse gas emissions. Efficient production of OME is a major focus of recent research, e.g. [10–19]

HVO are produced from triglyceride acids obtained from plants such as oilseed rape, and are often designated simply as “oils”. HVO contain mainly n-alkanes, but also some branched alkanes, with C-numbers typically between 15 and 20, but basically no sulfur, nitrogen, or aromatics. [4,20–23] HVO have similar physical properties as fossil diesel, but higher cetane numbers and lower toxic emissions. [24,25] It can be used directly as a diesel substitute without any modification of the engine. Only at low temperatures, the high viscosity can cause problems in some cases. [25]

HVO are already produced on a large scale, whereas there are only a few facilities for OME production. The use of blends of (OME + HVO) is of great interest for a market launch of OME. [4,19,26]

One problem with the application of blends of (OME + HVO) is the miscibility [3,18,27–29]. HVO are non-polar, while OME are moderately polar, due to the oxygen in the backbone. This can induce a miscibility gap in mixtures of (OME + HVO), which, however, is typically not large and can be avoided by a suitable choice of the composition. This is mandatory for the application as fuels, where homogeneity of the fluid is required. However, it is known that initially homogeneous mixtures of (OME + HVO) show a liquid-liquid phase split after some time in many technical applications. Typically, not only a small amount of the second phase is formed, but the amounts of both phases can be of the same order of magnitude, with one phase being OME-rich and the other HVO-rich. Only qualitative information on this phenomenon is available in the literature [3,18,27–29] and its reasons are not fully understood. A hypothesis is that the initially homogeneous (OME + HVO) mixture takes up small amounts of water from the air, which induces the phase split – however not by forming a (small) second water-rich phase, but by leading to a separation of OME and HVO.

70 This phenomenon was studied in the present work by phase equilibrium experiments, in which
71 liquid-liquid equilibria (LLE), as well as liquid-liquid-liquid equilibria (LLLE), were measured,
72 and by accompanying modeling and simulation. A challenge in designing a such study is that both
73 HVO and technical OME are mixtures. The composition of HVO depend on the raw material and
74 production process, and also the composition of technical OME varies. We have therefore decided
75 to carry out experiments with model components. Two OME were used: OME_4 because it is in the
76 middle of the typical range of OME_n components in OME-fuels (OME_3 – OME_5). Additionally,
77 we have also included OME_2 in the study, to get information on the influence of the chain length
78 of the OME_n on the results. Longer OME_n were not used, as they were not available in sufficient
79 amounts as pure components. As model component for HVO, n-hexadecane was used. Also here,
80 the influence of the chain length on the results was investigated by including n-dodecane in the
81 study. Longer n-alkanes were not studied to avoid experimental problems with solid-precipitation
82 at room temperature. Hence, LLE and LLLE in well-defined binary and ternary mixtures of the
83 type (OME_n + n-alkane + water) were studied.
84 Additionally, also an OME-mixture, as it is used in fuels, was included in the study. Furthermore,
85 also mixtures containing toluene were investigated, to see whether problems with de-mixing could
86 also occur in mixtures of OME with fossil diesel fuel, which contains considerable amounts of
87 aromatic hydrocarbons, in contrast to HVO.
88 There are only a few studies in the literature on LLE in the systems that are of interest here,
89 Table 1 gives an overview.
90
91

Table 1 Overview of experimental studies of LLE in systems that are related to the ones studied in the present work.

system	source
OME_n + water	Schmitz et al. [30]
n-alkanes + water	Mokbel et al. [31]
n-alkanes + water	Sutton et al. [32]
OME_n + n-hexane + water	Zhuang et al. [33]
OME_3 + (n-heptane, p-xylene, toluene) + water	Shi et al. [34]
OME_1 + (cyclohexane, n-heptane) + water	Shi et al. [35]
OME_n + o-xylene + water	Li et al. [36]
OME_n + toluene + water	Li et al. [37]

In none of these studies, a phase split between OME and hydrocarbons was observed. The present work is the first in which this phenomenon is studied in detail, in particular regarding the important influence of water.

Modeling LLE in mixtures containing small, highly polar components, such as water, and large non-polar or weakly polar components (as the n-alkanes and OME studied here) is challenging. We have tried two options: modeling with molecular equations of state (EOS), namely PC-SAFT [38,39], and modeling with UNIFAC [40], a group-contribution model of the Gibbs excess energy. In both cases, the model parameters were fitted to the experimental data. The latter is distinctly simpler and, as preliminary tests with PC-SAFT indicated no advantages, we have decided to continue only with UNIFAC, and report here on the results, which were obtained with this method. The UNIFAC model enables predictions of the complex phase behavior of the studied ternary systems, some of which show not only LLE but also liquid-liquid-liquid equilibria (LLLE).

There are only two modeling and simulation studies of related systems in the literature, in which, however, other models were used. Recently, Yang et al. [41] carried out a simulation study on the miscibility of OME_n with model components of diesel fuel using the COSMO-RS method. [42]

Yu et al. [43] investigated the miscibility of OME with diesel fuel components using molecular dynamics simulations. These simulation studies focus on similar systems like the already mentioned experimental studies and do not mention the phase split between OME and hydrocarbons or they are predictive and show no experimental proofs.

2. Experimental Apparatus and Procedure

2.1 Chemicals

OME_2 and OME_4 were provided by BASF SE with a purity of 0.985 g g^{-1}. The main impurities are minor amounts of shorter OME, which were identified using the NMR method from Breitkreuz et al. [44]. As they are only present in small amounts and chemically similar to the main component, the influence of these impurities on the results is expected to be only minor. The OME-mixture was provided by ASG Analytik-Service. The OME-mixture comprised OME_3 (0.58 g g^{-1}), OME_4 (0.27 g g^{-1}), OME_5 (0.11 g g^{-1}), and OME_6 (0.04 g g^{-1}). n-dodecane (C12), purity > 0.99 g g^{-1}, was purchased from ThermoFisher. n-hexadecane (C16), purity > 0.99 g g^{-1}, and toluene (Tol), purity > 0.998 g g^{-1}, were purchased from Merck. The purified water (specific resistance > 15 $M\Omega cm^{-1}$) was prepared with a Milli-Q system from Merck Millipore.

2.2 Phase equilibrium measurements

For the measurement of LLE, feed mixtures of different compositions were prepared from the pure components, except for the feed mixtures with low water fraction, for which not pure water

but OME was used that was saturated with water at 293 K. Where appropriate, OME was dried with molecular sieve (3A) before use. For the preparation of the feed mixtures, an analytical balance (AG 204, Mettler Toledo) was used and the composition was calculated based on the masses of the pure substances.

For the measurements at 293 K, 20 g of the feed mixture was filled into a glass vial which contained a magnetic stir bar, and was closed with a septum cap. The closed vial was stored in an air-thermostatted cabinet on a magnetic stir plate. The mixture was stirred for at least 24 hours. Then, the stirrer was turned off and the phases were allowed to settle for at least 48 hours. These values were chosen based on preliminary experiments, which showed that a further prolongation did not yield significantly different results. Subsequently, samples of the different phases were taken with syringes through the septum. Before use, the syringes were dried in an exsiccator that was filled with dried molecular sieve for at least 48 hours. The temperature was measured in the cabinet with a calibrated platinum resistance thermometer. In preliminary experiments, in which the temperature was also measured in a vial, the maximal temperature difference between the air and the vial was measured. The overall uncertainty of the reported temperature in the vial is estimated to be 0.1 K.

For the measurements at 278 and 265 K, 40 g of the feed mixture was filled into a glass vial with a cooling jacket, which, in turn, was isolated from the surroundings by a vacuum jacket. The vial was equipped with a magnetic stir bar. The cooling medium was a mixture of water and monoethylene glycol and was thermostatted with a cryostat. The temperature inside the vial was measured with a platinum resistance thermometer (uncertainty of 0.1 K). The times for mixing and settling were the same as in the measurements at 293 K. After the settling period samples from the

different phases were taken through septa which are located at different heights of the vial. For the sampling dried syringes were used.

All experiments were carried out at ambient pressure (1 bar ± 0,05 bar); as only equilibria with liquid phases were studied variations of the pressure have no significant influence on the results. This could, however, be different for the pressures used in injection systems in diesel engines, which can be more than 1000 bar. No replica measurements were done, as the number of experiments for each studied system was large enough to check the quality of the data by considering their continuity.

2.3 Chemical Analysis

Only the samples from the coexisting phases were analyzed. The composition of the feed was known from the gravimetric preparation. The uncertainty of the feed composition is better than 0.001 g g^{-1}.

All samples were first analyzed with quantitative ^{1}H-nuclear magnetic resonance (NMR) spectroscopy to determine the concentrations of OME, water, and the hydrocarbons. The equipment was the same as described by Breitkreuz et al. [44] The acquisition parameters were the following: flip angle: 90°, acquisition time: 4 s, repetition time: 20 s, 8 scans, and 65 k data points. The peak assignment was done in preliminary studies based on experiments with pure components and mixtures. For the evaluation of the spectra, the software MestReNova 14.2 was used and it was assumed that the proportionality constant relating the peak area to the amount of substance is the same for all peaks. Sample spectra and the peak assignment are reported in the Supporting Information. Results from test measurements with samples that were prepared

gravimetrically showed that the uncertainty for the results for the concentrations of the different components does not exceed 0.01 mol mol^{-1}. For the measurements with the OME-mixture, additionally ^{13}C NMR spectroscopy was used to avoid problems with peak overlaps. The procedure was adopted from Breitkreuz et al. [44] For samples with water-contents below 0.1 g g^{-1}, additionally, Karl-Fischer titration was used to determine the water concentration (for mass fractions in the range of 0.1 to 0.005 g g^{-1} volumetric Karl-Fischer titration and below 0.005 g g^{-1} coulometric Karl-Fischer titration). Each titration was carried out at least three times and the mean value was used as the result. The uncertainty of the Karl-Fischer titration results for the water concentration is estimated to be 80 ppm for the coulometric titration and 0.001 g g^{-1} for volumetric titration, based on experiments with gravimetrically prepared samples. Further information on the Karl-Fischer titration is given in the Supporting Information. When Karl-Fischer titration results were available, they were used and the NMR results were neglected.

3. Modeling

The phase equilibria were calculated using the isoactivity criterion in Equation 1 which is given here for LLLE.

$$x_i' \cdot \gamma_i' = x_i'' \cdot \gamma_i'' = x_i''' \cdot \gamma_i''', \; i = 1 \ldots N \tag{1}$$

Therein is x_i the mole fraction of component i and γ_i the corresponding activity coefficient; N is the number of components in the mixture and the primes refer to the phases. The activity coefficient was calculated with the group contribution model UNIFAC with parameters from Schmitz et al. [45], or, where this was not possible, from the original UNIFAC model [46]. Furthermore, group interaction parameters representing interactions between groups in OME and

in hydrocarbons were fitted to experimental results from the present work. Details on the parameterization are reported in the Supporting Information. The split of the considered components into UNIFAC groups is reported in Table 2, the group parameters, and the interaction parameters in Table 3. Tables 2 and 3 also contain detailed information on the source of all parameters. As the activity coefficients calculated with UNIFAC depend only on a temperature and composition, the model does not account for the pressure.

Table 2 Group assignment and size and surface parameters of the groups for the UNIFAC-based activity coefficient model.

Comp. *i*	group	count	R_i	Q_i	Ref.
OME_n	MAL	1	2.9644	2.7160	[45]
	FA_{OME}	(*n*-1)	0.9183	0.7800	[45]
C12	CH_3	2	0.9011	0.8480	[47]
	$CH_{2,alk}$	10	0.6744	0.5400	[45]
C16	CH_3	2			
	$CH_{2,alk}$	14			
Tol	ACH	5	0.5313	0.4000	[47]
	$ACCH_3$	1	1.2663	0.9680	[47]
W	H_2O	1	0.9200	1.4000	[45]

Table 3 Group interaction parameters for the UNIFAC activity coefficient model.

group *j* → group *i* ↓	MAL	FA_{OME}	CH_3 / CH_2	ACH	$ACCH_3$	H_2O
MAL	-	26.0[a]	-45.522 [c]	-103.618 [c]	-45.522[c]	1031.0-1.749 · T/K [a]
FA_{OME}	141.5 [a]	-	265.483 [c]	52.13 [b]	265.48[c]	670.7 [a]
CH_3 / CH_2	51.251 [c]	148.309 [c]	-	61.13 [b]	76.5 [b]	1318 [b]
ACH	6400.299 [c]	32.14 [b]	-11.12 [b]	-	167.0 [b]	903.8 [b]
$ACCH_3$	51.251 [c]	148.309 [c]	-69.7 [b]	-146.8 [b]	-	5695.0 [b]
H_2O	-225.5+0.7205·T/K [a]	168.9-0.8776·T/K [a]	300 [b]	362.3 [b]	377.6 [b]	-

[a]Schmitz et al. [45] [b]Gmehling et at. [47] [c]this work

Isothermal flash calculations were used to determine the two-phase and the three-phase equilibria studied in the present work. The feed composition for the flash-calculation was calculated from the experimental phase compositions assuming an equimolar phase split and the initial guess for the algorithm was calculated with the method of Ohanamah and Thompson [48]. The flash model was implemented in the software Matlab. Details on the calculation can be found in the Supporting Information.

4. Results and discussion

4.1 Overview

Before the experimental and model results are presented, we discuss the topologies of the corresponding phase diagrams. Both the experimental results and the model show that there are three types of phase diagrams in the systems studied here (in the temperature range that was investigated). The three topologies, labeled here as type A, B, and C, respectively, are depicted in Figure 1.

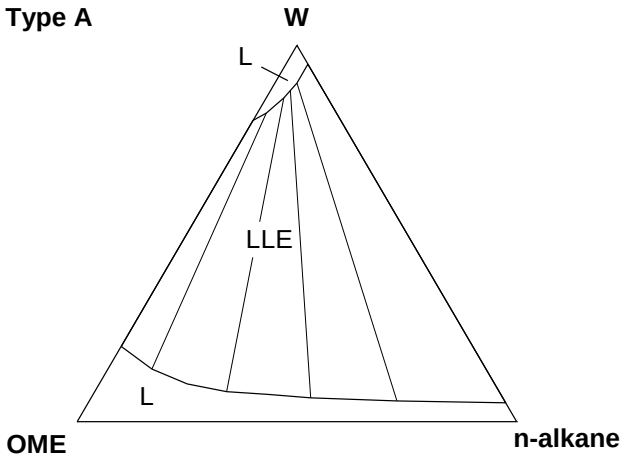
Type A
W
L
LLE
L
OME
n-alkane

230

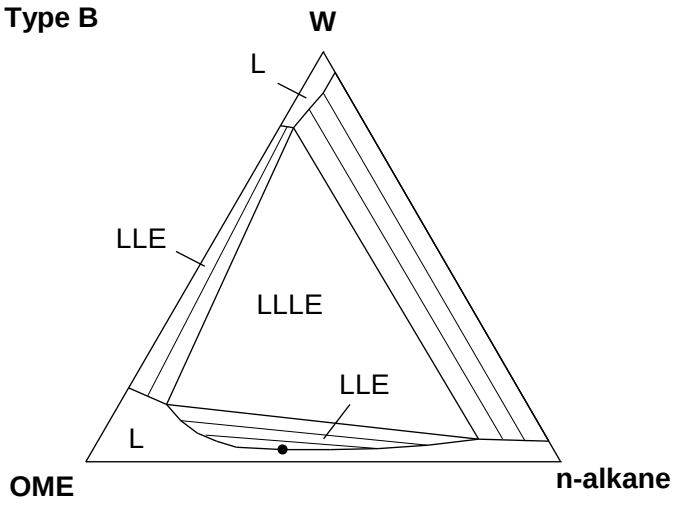
Type B
W
L
LLE
LLLE
LLE
L
OME
n-alkane

231

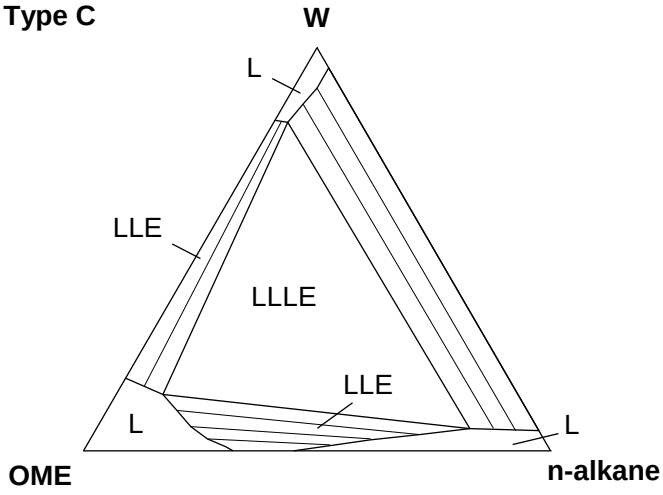
Type C
W
L
LLE
LLLE
LLE
L
L
OME
n-alkane

232

Figure 1: Schematic representation of the three topologies of the phase behavior of the systems studied in this work. The straight lines represent LLE conodes. The point mark in the type B diagram is a critical point.

Type A was observed in all experiments with OME_2: OME_2 and the n-alkanes are completely miscible, while there are miscibility gaps in the binary systems with (OME_2 + water) and (n-alkane + water). A ternary LLE region connects these two binary LLE.

In the type C phase diagram, there is also a miscibility gap in the binary system (OME + n-alkane). This is the case for (OME_4 + C16) for all temperatures and (OME_2 + C16) for the two lower studied temperatures (278 and 265 K). In the ternary system, there are three (two-phase) LLE regions that stretch out from the binary sides of the phase diagram and meet in a (three-phase) LLLE in the center of the diagram

Type B phase diagram has features from the other two types, which are, however, combined differently. As in the type C phase diagram, there is a (three-phase) LLLE. On the three sides of this LLLE-region, there are two phase LLE regions. However, only two of them are connected to binary sides of the phase diagram, whereas the third one, that on the side with low water concentrations, ends in a critical point, as there is no miscibility gap on the (OME + n-alkane) side of the phase diagram. This phase behavior was observed in the system (OME_4 + C12) at the highest studied temperature 293 K.

For some of the studied systems and temperatures, it is not possible to decide whether the phase behavior is of type B or C. An overview of the assignments of systems and temperatures to the phase behavior is given in Table 4.

The phenomenon of the unexpected phase split in technical mixtures of OME and HVO is very likely related to the occurrence of phase behavior of type B, cf. Figure 1. In the absence of water,

OME and HVO are completely miscible. However, upon taking up water, the closed LLE region is reached and the mixture splits up into a OME-rich phase and a HVO-rich phase. If larger amounts of water are added (more than is usually taken up from the air), the three-phase region is reached and an additional third, water-rich phase forms.

Table 4 Overview of the systems studied in this work. The third or fourth component was always water.

OME	Hydrocarbon	Temperature / K	Number of feed mixtures	Topology type
OME_2	C12	293	6	A
		278	4	A
	C16	293	6	A
OME_4	C12	293	5	B
		278	5	C
		265	4	C
	C16	293	5	C
	C16 + Tol		3	B or C[a]
OME_{mix}	C12	293	1	B or C[a]
	C16		1	B or C[a]

[a] not clarified

4.2 Experiments in the system (OME + n-alkane + water)

First, the experimental results for the model systems are presented, in which the chain length of the alkanes and OMEs and the temperature were systematically varied. Then, the fit of the model to these results is then discussed. The numerical results are presented in Tables 5 to 8. The data for each system are grouped in isothermal subsets. In some of these sets, the temperature was only

271 constant to about 1 K, which was due to problems with the setting of the temperature. The
272 uncertainty of the reported individual values is as specified above.

273 **Table 5** Experimental LLE data for the system (OME_2 + C12 + water). The composition of the
274 feed is reported in the Supporting Information. Standard uncertainties u are $u(T)$=0.1 K,
275 $u(\tilde{x}_{\mathrm{OME2}})$=0.01 mol mol^{-1}, $u(\tilde{x}_{\mathrm{C12}})$=0.01 mol mol^{-1}, $u(\tilde{x}_{\mathrm{W}})$=0.01 mol mol^{-1} (for 0.005 g g^{-1} < $\tilde{x}_{\mathrm{W}}^{(m)}$ <
276 0.1 g g^{-1}: $u(\tilde{x}_{\mathrm{W}}^{(m)})$=0.001 g g^{-1} and for $\tilde{x}_{\mathrm{W}}^{(m)}$<0.005 g g^{-1}: $u(\tilde{x}_{\mathrm{W}}^{(m)})$=0.00008 g g^{-1})

277

T / K	water-rich phase		organic phase	
	$x_{\mathrm{W}}^{(\mathrm{m})}$ g g^{-1}	$x_{\mathrm{OME2}}^{(\mathrm{m})}$ g g^{-1}	$x_{\mathrm{W}}^{(\mathrm{m})}$ g g^{-1}	$x_{\mathrm{OME2}}^{(\mathrm{m})}$ g g^{-1}
264.37	solid[a]		0.0008	0.3290
278.28	0.8123	0.1870	0.0002	0.1323
278.50	0.7219	0.2781	0.0024	0.4496
278.71	0.7082	0.2918	0.0058	0.6421
293.15	0.7054	0.2946	0.0153	0.8029
	0.7122	0.2878	0.0113	0.7349
	0.7542	0.2458	0.0018	0.3648
	0.7970	0.2030	0.0012	0.2209
	0.7313	0.2687	0.0046	0.5420
	0.8354	0.1646	0.0003	0.1231

[a]not analyzed

278

279

280

281

282

283

Table 6 Experimental LLE data for the system (OME_2 + C16 + water). The composition of the feed is reported in the Supporting Information. Standard uncertainties u are $u(T)$=0.1 K, $u(\tilde{x}_{OME2})$=0.01 mol mol^{-1}, $u(\tilde{x}_{C16})$=0.01 mol mol^{-1}, $u(\tilde{x}_{W})$=0.01 mol mol^{-1} (for 0.005 g g^{-1} < $\tilde{x}_{W}^{(m)}$< 0.1 g g^{-1}: $u(\tilde{x}_{W}^{(m)})$=0.001 g g^{-1} and for $\tilde{x}_{W}^{(m)}$<0.005 g g^{-1}: $u(\tilde{x}_{W}^{(m)})$=0.00008 g g^{-1})

T / K	water-rich phase		organic phase	
	$x_{W}^{(m)}$ / g g^{-1}	$x_{OME2}^{(m)}$ / g g^{-1}	$x_{W}^{(m)}$ / g g^{-1}	$x_{OME2}^{(m)}$ / g g^{-1}
293.15	0.7132	0.2868	0.0105	0.6971
	0.7023	0.2978	0.0116	0.7152
	0.7021	0.2979	0.0067	0.5991
	0.7229	0.2771	0.0032	0.4389
	0.7577	0.2423	0.0010	0.2568
	0.8483	0.1517	0.0003	0.1145

Table 7 Experimental LLE and LLLE data for the system (OME_4 + C12 + water). The composition of the feed is reported in the Supporting Information. Standard uncertainties u are $u(T)$=0.1 K, $u(\tilde{x}_{OME4})$=0.01 mol mol^{-1}, $u(\tilde{x}_{C12})$=0.01 mol mol^{-1}, $u(\tilde{x}_{W})$=0.01 mol mol^{-1} (for 0.005 g g^{-1} < $\tilde{x}_{W}^{(m)}$< 0.1 g g^{-1}: $u(\tilde{x}_{W}^{(m)})$=0.001 g g^{-1} and for $\tilde{x}_{W}^{(m)}$<0.005 g g^{-1}: $u(\tilde{x}_{W}^{(m)})$=0.00008 g g^{-1})

T / K	water-rich phase		alkane-rich phase		OME-rich phase	
	$x_{W}^{(m)}$ g g^{-1}	$x_{OME4}^{(m)}$ g g^{-1}	$x_{W}^{(m)}$ g g^{-1}	$x_{OME4}^{(m)}$ g g^{-1}	$x_{W}^{(m)}$ g g^{-1}	$x_{OME4}^{(m)}$ g g^{-1}
264.27	solid[a]		0.0001	0.1418	0.0131	0.9372
265.63			0.0001	0.1537	0.0094	0.9339
266.71			0.0001	0.1643	0.0040	0.9254
266.78			0.0008	0.1716	0.0021	0.9220
267.19			0.0002	0.1592	0.0076	0.9282
278.63	0.7542	0.2457	0.0004	0.1953	0.0178	0.9166
278.41			0.0004	0.2217	0.0092	0.9042
278.43			0.0003	0.2413	0.0054	0.8922
278.84			0.0004	0.2057	0.0144	0.9133

Table 7 continued

278.86			0.0002	0.2599	0.0027	0.8783
293.15	0.7691	0.2309	0.0011	0.2753	0.0214	0.8918
293.15			0.0011	0.3950	0.0051	0.8097
293.15			0.0011	0.3346	0.0087	0.8510
293.15			0.0011	0.2796	0.0122	0.8721

[a] not analyzed

293

294 **Table 8** Experimental LLE and LLLE data for the system (OME_4 + C16 + water). The composition
295 of the feed is reported in the Supporting Information. Standard uncertainties u are $u(T)$=0.1 K,
296 $u(\tilde{x}_{OME4})$=0.01 mol mol^{-1}, $u(\tilde{x}_{C16})$=0.01 mol mol^{-1}, $u(\tilde{x}_{W})$=0.01 mol mol^{-1} (for 0.005 g g^{-1} < $\tilde{x}_{W}^{(m)}$ <
297 0.1 g g^{-1}: $u(\tilde{x}_{W}^{(m)})$=0.001 g g^{-1} and for $\tilde{x}_{W}^{(m)}$<0.005 g g^{-1}: $u(\tilde{x}_{W}^{(m)})$=0.00008 g g^{-1})

T / K	water-rich phase		alkane-rich phase		OME-rich phase	
	$x_{W}^{(m)}$ / g g^{-1}	$x_{OME4}^{(m)}$ / g g^{-1}	$x_{W}^{(m)}$ / g g^{-1}	$x_{OME4}^{(m)}$ / g g^{-1}	$x_{W}^{(m)}$ / g g^{-1}	$x_{OME4}^{(m)}$ / g g^{-1}
293.15	0.74974	0.25026	0.0005	0.1666	0.0279	0.9378
			0.0005	0.1815	0.0182	0.9553
			0.0004	0.1975	0.0110	0.9419
			0.0002	0.2235	0.0035	0.9180
			0.0002	0.2352	0.0004	0.8770

298 In Figure 2, the LLE in the systems (OME_2 + C12 + water) and (OME_2 + C16 + water) are shown.
299 The different temperatures are indicated by different colors and the symbol type indicates the
300 n-alkane that was used. The feed compositions for the different tie lines are shown as crosses.

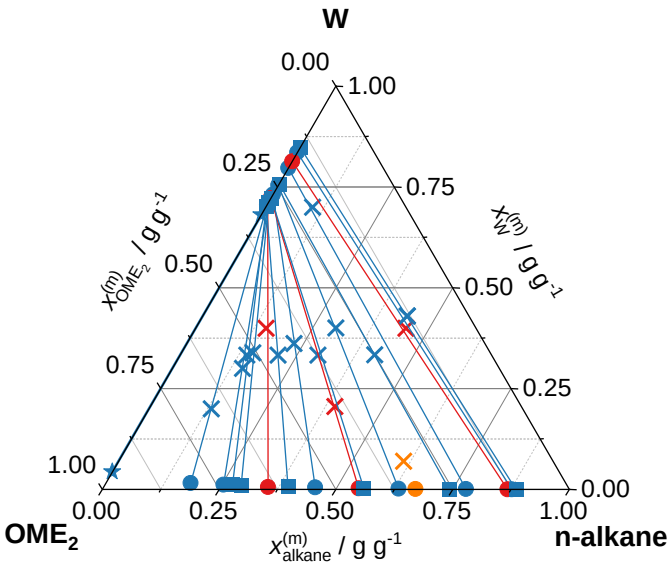

Figure 2: Experimental results for the LLE in the system (OME_2 + C12 + water, circles) and the system (OME_2 + C16 + water, squares). The color indicates the temperature: (blue) 293 K, (red) 278 K, (orange) 265 K. Stars indicate data from Schmitz et al.[30] for the binary system (OME_2 + water). Crosses represent the feed compositions. Lines are tie lines. For the measurement at 278 K, only one liquid phase could be measured due to ice formation.

It can be seen that the feed compositions lie perfectly on the tie lines, indicating a good quality of the experimental results. In all experiments, a split into a water-rich phase and an organic phase was observed. In the water-rich phase, no n-alkane was found. The concentration is so small that it is below the detection limit of the NMR-measurement. This is consistent with reports from the literature [31,32] for the solubility of C12 and C16 in pure water, which does not exceed 0.1 ppm.

The OME fraction in the water-rich phase increases with increasing ratio of OME_2/n-alkane in the feed and approaches the value for the system (OME_2 + water) from Schmitz et al. [30], which is also indicated in Figure 2. There is no data for the composition of the water-rich phase at 265 K,

for which only the organic liquid phase could be analyzed, due to ice formation. The resolution of the presentation of the data in Figure 2 is too low to discern an influence of the temperature or the type of n-alkane.

Therefore, the results for the composition of the organic phase, which is of special interest for fuel applications, are shown separately in Figure 3. Additionally, also the experimental data from Zhuang et al. [33] for the system (OME_2 + n-hexane + water) are shown.

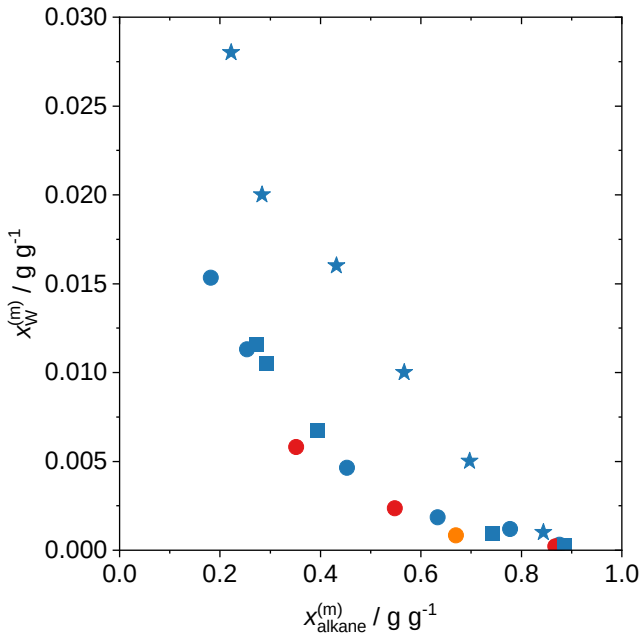

Figure 3: Experimental results for the composition of the organic phase in LLE in the system (OME_2 + C12 + water, circles) and the system (OME_2 + C16 + water, squares). The color represents the temperature: (blue) 293 K, (red) 278 K, (orange) 265 K. Stars indicate data from Zhuang et al.[33] for the system (OME_2 + n-hexane + water).

As expected, the concentration of water increases with increasing amount of OME_2 (decreasing amount of the n-alkane). The differences between the different data sets from the present work are not large (as could be expected from Figure 2) but indicate a tendency for an increasing water

329 amount with increasing temperature, which is also not unexpected, due to the weaker influence of
330 H-bonds at higher temperatures. The differences between the results for C12 and C16 are basically
331 within the scattering of the data. The results of Zhuang et al [33] for the system (OME_2 + n-hexane
332 + water) at 292 K show significantly higher water solubilities in the organic phase than the results
333 from the present work that were, however, obtained with longer n-alkanes.
334 The LLLE measured in the systems (OME_4 + C12 + water) and (OME_4 + C16 + water) are shown
335 in Figure 4. For (OME_4 + C12 + water), results for different temperatures are presented.
336 The variation of the temperature and alkane hardly affects the water-rich phase (that contains
337 practically no alkane) and has only a moderate influence on the OME_4-rich phase. A stronger
338 influence is observed for the alkane-rich phase.
339 This is discussed in more detail using Figure 5, which shows results for the two organic phases of
340 the LLLE together with results for the LLE in the region with low water concentrations (cf.
341 Figure 1).
342 All results shown in Figure 5 belong to the type C phase behavior, except those for the system
343 (OME_4 + C12 + water) at 293 K, which has type B phase behavior.

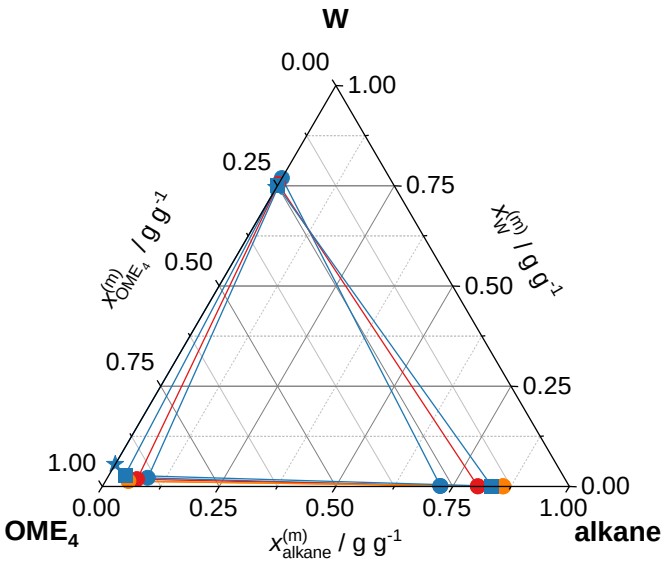

344

345 **Figure 4:** Experimental results for the LLLE in the system (OME_4 + C12 + water, circles) and the

346 system (OME_4 + C16 + water, squares). The color represents the temperature: (blue) 293 K, (red)

347 278 K, (orange) 265 K. Stars indicate data from Schmitz et al.[30] for the binary system (OME_4 +

348 water). Lines are tie lines.

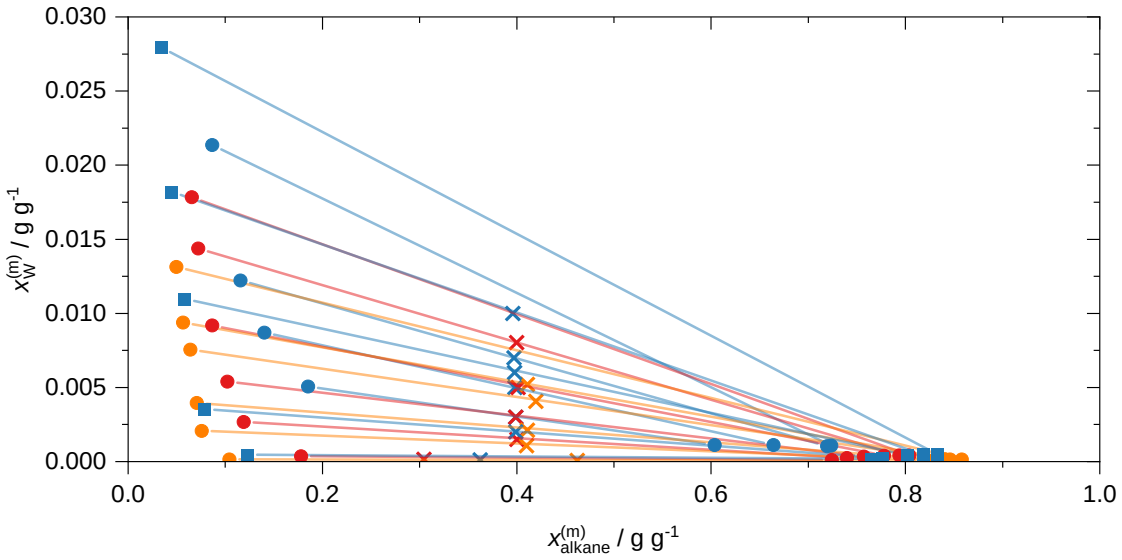

349

Figure 5: Experimental results for the LLE in the system (OME_4 + C12 + water, circles) and the system (OME_4 + C16 + water, squares) at low water fractions. The color represents the temperature: (blue) 293 K, (red) 278 K, (orange) 265 K. Crosses represent the feed compositions. Lines are tie lines. The top results for each temperature and alkane represent the phases with low water fractions of the LLLE.

Figure 5 shows that decreasing the temperature leads to a widening of the LLE region, i.e. to an increasing mole fraction of OME_4 in the OME_4-rich phase as well as an increasing mole fraction of C12 in the C12-rich phase. The water-content in the alkane-rich phase is always very low; it increases with increasing OME-content of that phase (not discernable in Figure 5). Water from the feed is basically only found in the OME_4-rich phase. Also the increase in the chain-length of the n-alkane from C12 to C16 increases the width of the miscibility gap. Again, the feed concentrations lie on the LLE tie-lines.

In the present work, the type A phase behavior was only observed for OME_2. Zhuang et al. [33] mixed OME_4 with the smaller alkane n-hexane and also observed type A phase behavior. Type B phase behavior can be considered as an intermediate between types A and C, the difference is mainly caused by the differences in the solubility of the binary system (OME + n-alkane).

4.3 Modeling of the system (OME + n-alkane + water)

In the following, modeling results are compared to experimental results in figures that are similar to Figures 2 to 5. However, for the comparison, mole fractions are used, which enables a better resolution of differences than the mass fractions used in Figures 2 to 5, which were preferred in

these figures, as they are more convenient for applications. We have refrained from presenting the modeling results already in Figures 2 to 5, to avoid an overloading with information.

In Figure 6, the experimental results for the LLE in the studied systems of the type (OME_2 + n-alkane + water) are compared to the results from the model and Figure 7 shows the corresponding results for the LLLE in the system of the type (OME_4 + n-alkane + water). The modeling results for these two systems in plots that are similar to the ones shown in Figures 4 and 5 are shown in the Supporting Information.

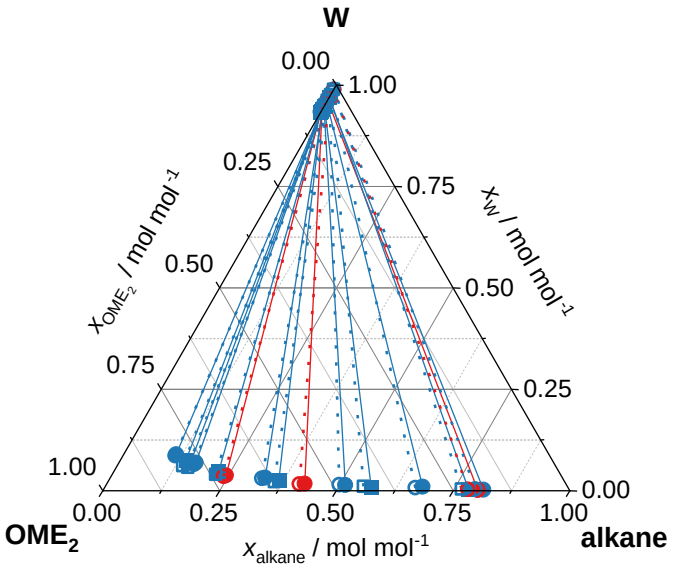

Figure 6: Experimental results (filled symbols and full line) and model results (open symbols and dashed line) for the LLE in the system (OME_2 + C12 + water, circles) and the system (OME_2 + C16 + water, squares). The color represents the temperature: (blue) 293 K, (red) 278 K. Lines are tie lines.

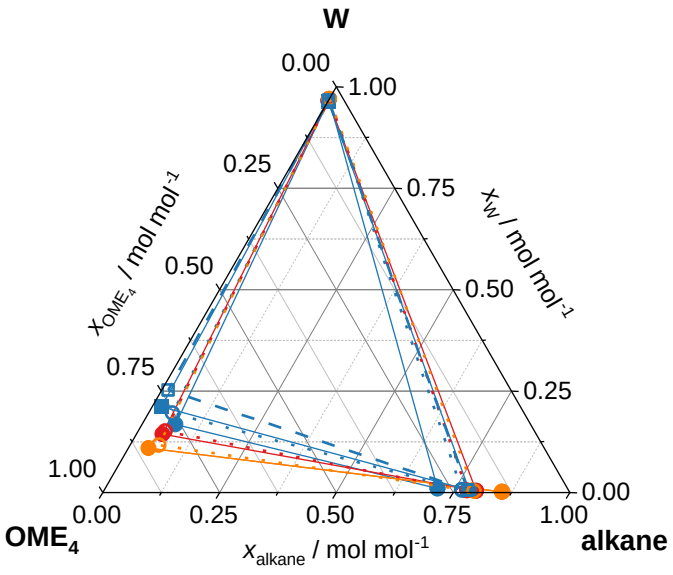

385

386 **Figure 7:** Experimental results (filled symbols and full line) and model results (open symbols and
387 dashed line) for the LLLE in the system (OME_4 + C12 + water, circles) and the system (OME_4 +
388 C16 + water, squares). The color represents the temperature: (blue) 293 K, (red) 278 K, (orange)
389 265 K.

390 The model confirms the topologies A to C discussed above. The water-rich phase is described
391 well in all cases. The water mole-fraction in the OME-rich phase is overestimated and the width
392 of the miscibility gap between the OME-rich and the alkane-rich phase is underestimated, but the
393 trends regarding the influence of the temperature and alkane chain length are described correctly.

394

395

396

397

398

4.4 Experiments with systems with more than three components

4.4.1 System (OME_4 + C16 + Tol + water)

LLLE in mixtures of (OME_4 + C16 + Tol + water) were studied at 293 K. In the experiments, the ratio OME_4/(C16 + Tol)/water was held constant, and only the ratio C16/Tol was varied. The feed composition was chosen so that the resulting mixture split into three phases. The numerical results are presented in Table 9. The results are discussed here using ternary phase diagrams, in which Tol and C16 were lumped into a single component.

Figure 8 shows the experimental results together with those for the Tol-free system. Besides the experimental data also the results from the model are depicted.

Table 9 LLE data of the system (OME_4 + C16 + Tol + water) at 293.15 K. The composition of the feed is reported in the Supporting Information. Standard uncertainties u are $u(T)$=0.1 K, $u(\tilde{x}_{OME4})$=0.01 mol mol^{-1}, $u(\tilde{x}_{hydrocarbon})$=0.01 mol mol^{-1}, $u(\tilde{x}_W)$=0.01 mol mol^{-1} (for 0.005 g g^{-1} < $\tilde{x}_W^{(m)}$< 0.1 g g^{-1}: $u(\tilde{x}_W^{(m)})$=0.001 g g^{-1} and for $\tilde{x}_W^{(m)}$<0.005 g g^{-1}: $u(\tilde{x}_W^{(m)})$=0.00008 g g^{-1})

water-rich phase			(C16 + Tol)-rich			OME-rich phase		
$x_W^{(m)}$ / g g^{-1}	$x_{OME4}^{(m)}$ / g g^{-1}	$x_{Tol}^{(m)}$ / g g^{-1}	$x_W^{(m)}$ / g g^{-1}	$x_{OME4}^{(m)}$ / g g^{-1}	$x_{Tol}^{(m)}$ / g g^{-1}	$x_W^{(m)}$ / g g^{-1}	$x_{OME4}^{(m)}$ / g g^{-1}	$x_{Tol}^{(m)}$ / g g^{-1}
0.7573	0.2428	0.00000	0.0005	0.1722	0.0125	0.0262	0.9281	0.0091
0.7592	0.2408	0.00000	0.0006	0.1850	0.0280	0.0239	0.9119	0.0218
0.8886	0.1114	0.00000	0.0016	0.2285	0.3329	0.0140	0.7644	0.1298

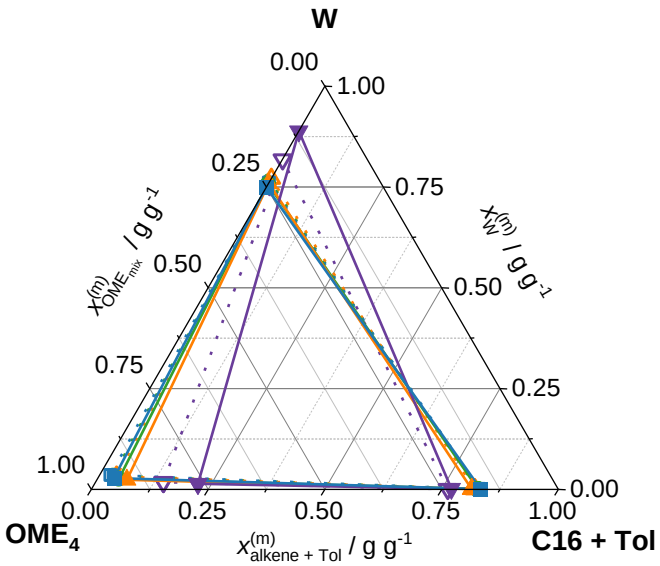

416

417 **Figure 8:** Experimental results (filled symbols and straight line) and model results (open symbols
418 and dashed line) for the LLLE in the system (OME_4 + C16 + Tol + water) at 293.15 K. Tol and
419 C16 are lumped in the representation. Results from experiments with varying ratios of Tol/C16
420 are shown. The mass fractions of Tol in the (C16 + Tol) feed mixture ($x^{(m)}_{Tol,mix}$) were: (blue
421 squares) $x^{(m)}_{Tol,mix}$ = 0.0 g g^{-1}, (green circles) $x^{(m)}_{Tol,mix}$ = 0.02 g g^{-1}, (orange upwards
422 triangle) $x^{(m)}_{Tol,mix}$ = 0.05 g g^{-1}, (purple downwards triangle) $x^{(m)}_{Tol,mix}$ = 0.2 g g^{-1}.

423 In the Tol-containing systems, the basic findings regarding the three phases are the same as for
424 the Tol-free system. Upon increasing the amount of Tol, the amount of water in the water-rich
425 phase increases and the miscibility gap between the hydrocarbon-rich phase and the OME-rich
426 phase gets smaller, i.e., Tol acts as a solubilizer. This can be attributed to a mediating influence of
427 the pi-electron systems of Tol. The model predicts these trends right but underestimates the

magnitude of the influence of Tol. A detailed analysis of the numerical results presented in Table 9 reveals that the ratio of C16/Tol in the different phases is similar, i.e., they do not separate.

4.4.2 Systems of the type (OME-mixture + n-alkane + water)

Measurements in systems containing a mixture of OME_3, OME_4, OME_5, and OME_6 of a fixed composition (OME_{mix}), water, and either C12 or C16 were carried out at 293.15 K. The feed was again chosen so that it was inside the three phase region. The numerical results for the LLLE are reported in Table 10 and are illustrated in Figure 9, which shows a ternary diagram, in which OME_3, OME_4, OME_5, and OME_6 are lumped into one pseudo-component OME_{mix}. Additionally, Figure 10 depicts the analytical results for the individual components in the three phases.

Table 10 Experimental LLLE data of systems of the type (OME_{mix} + alkane + water) at 293.15 K. OME_{mix} is a mixture of OME_3 to OME_6. The composition of the feed is reported in the Supporting Information. Standard uncertainties u are $u(T)$=0.1 K, $u(\tilde{x}_{OMEn})$=0.01 mol mol^{-1}, $u(\tilde{x}_{alkane})$=0.01 mol mol^{-1}, $u(\tilde{x}_{W})$=0.01 mol mol^{-1} (for 0.005 g g^{-1} < $\tilde{x}_W^{(m)}$< 0.1 g g^{-1}: $u(\tilde{x}_W^{(m)})$=0.001 g g^{-1} and for $\tilde{x}_W^{(m)}$<0.005 g g^{-1}: $u(\tilde{x}_W^{(m)})$=0.00008 g g^{-1})

alkane	phase	$x_W^{(m)}$ / g g^{-1}	$x_{alkane}^{(m)}$ / g g^{-1}	$x_{OME3}^{(m)}$ / g g^{-1}	$x_{OME4}^{(m)}$ / g g^{-1}	$x_{OME5}^{(m)}$ / g g^{-1}	$x_{OME6}^{(m)}$ / g g^{-1}
C16	OME-rich	0.0256	0.0923	0.3527	0.2872	0.1800	0.0622
	water-rich	0.7062	0	0.1664	0.1131	0.0102	0.0041
	alkane-rich	0.0004	0.7813	0.1112	0.0673	0.0292	0.0106
C12	OME-rich	0.0273	0.0922	0.3521	0.2866	0.1796	0.0621
	water-rich	0.7170	0	0.1371	0.0841	0.0470	0.0133
	alkane-rich	0.0013	0.7176	0.1417	0.0839	0.0434	0.0121

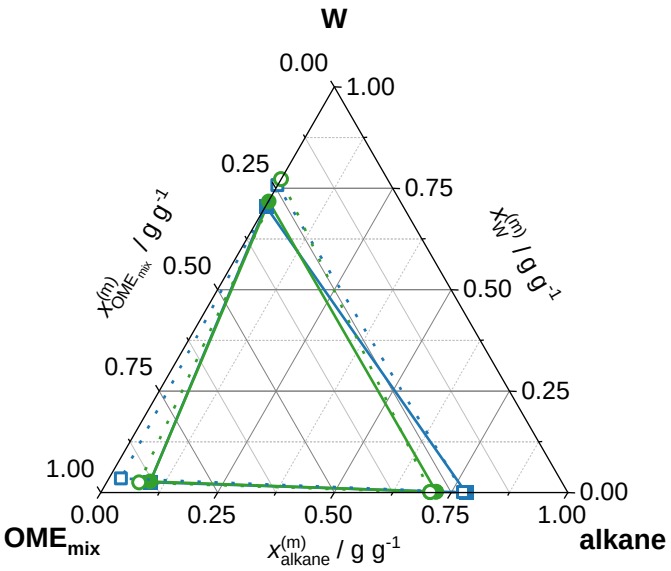

445

446 **Figure 9:** Experimental results (filled symbols and straight line) and model results (open symbols
447 and dashed line) for the LLLE in systems of the type (OME_{mix} + alkane + water) at 293 K. The
448 symbols represent the alkane: (circles) C12, (squares) C16.

449

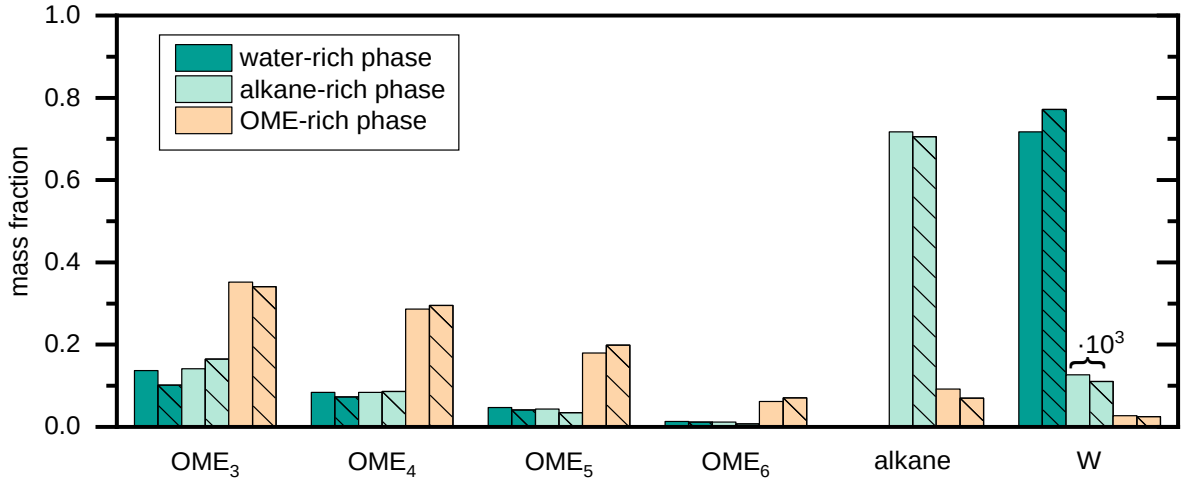

450

Figure 10: Results for LLLE in systems of the type (OME_{mix} + C12 + water) at 293 K. Experimental mass fractions (unhatched bars) are compared to mass fractions from the model (hatched bars) for all three phases. The water fraction in the C12-rich phase was multiplied by 1000 for a better visualization.

The experimental results are similar to those of the measurements with pure OME_4 (cf. Figure 4). The ratios OME_3 / OME_4 / OME_5 / OME_6 do not differ significantly in the different phases and are therefore also basically the same as in the feed mixture. All in all, the model shows a good agreement with the experimental data. The alkane-rich phase is described very well (cf. Figure 10). The distribution of the individual OME is also reproduced well by the model. The water fraction in the water-rich phase is somewhat underestimated.

5. Conclusions

Mixtures of poly(oxymethylene) dimethyl ethers (OME) and hydrogenated vegetable oil (HVO) are interesting synthetic fuels. However, in technical applications of these fuels, a liquid-liquid phase split was observed, which is unwanted. Up to now, only qualitative information on this phenomenon was available and its causes were unclear. The present work clearly indicates that the hypothesis that the phase separation is a consequence of the uptake of water from the air by the (OME + HVO) mixtures in many technical applications is correct. This leads to a separation into an OME-rich phase, which contains basically all the water, and a HVO-rich phase, which is almost water-free. This can be deduced from the results of the experimental studies on liquid-liquid equilibria (LLE) and liquid-liquid-liquid equilibria (LLLE) in model systems of the type (OME + alkane + water) that we have carried out in the present work.

Depending on the system and temperature, three different topologies of the phase behavior were observed. The unwanted liquid-liquid phase split is induced by a latent incompatibility of the OME with the alkane, which becomes only manifest when water is added. Furthermore, experiments with mixtures that contained not only alkanes but also toluene were carried out. The presence of the aromatic compound makes the alkane-rich phase more hydrophilic, and, hence, more compatible with OME. This reduces the risk of the phase split.

The experimental findings were also confirmed by simulations, in which UNIFAC, a model of the Gibbs excess energy, was used for describing the liquid phases. This comparatively simple modeling approach gave good results.

Now that the causes of the phase split are clear, measures to circumvent it can be found: a straightforward approach is to reduce the humidity in the fuel storage tank, e.g., by common drying agents, such as molecular sieves. Another approach is to add further fuel components that act as solubilizers. Ranked on a polarity scale, they should lie between OME_4 and the alkanes. The model developed in the present work can be used for a screening of such solubilizers.

Acknowledgements

The authors gratefully acknowledge funding by the German Federal Ministry of Economic Affairs and Energy within the project “E2Fuels” under Grant 19I18008F.

References

[1] Münz M, Mokros A, Beidl C. Analysis of two engine configurations using OME as a potential CO2-neutral and low emission diesel substitute. In: Liebl J, Beidl C, Maus W,

editors. Internationaler Motorenkongress 2019. Wiesbaden: Springer Fachmedien Wiesbaden; 2019, p. 369–384.
[2] Härtl M, Gaukel K, Pélerin D, Wachtmeister G. Oxymethylenether als potenziell CO2-neutraler Kraftstoff für saubere Dieselmotoren Teil 1: Motorenuntersuchungen. MTZ Motortech Z 2017;78(2):52–9. https://doi.org/10.1007/s35146-016-0170-9.
[3] Unglert M, Bockey D, Bofinger C, Buchholz B, Fisch G, Luther R et al. Action areas and the need for research in biofuels. Fuel 2020;268:117227. https://doi.org/10.1016/j.fuel.2020.117227.
[4] Holzer A, Guenthner M. Investigation of the Emission Reduction Potential of HVO-OME Fuel Blends in a Single-Cylinder Diesel Engine. In: SAE Technical Paper Series. Warrendale: SAE International; 2021.
[5] Münz M, Mokros A, Töpfer D, Beidl C. OME - Partikelbewertung unter Realfahrbedingungen. MTZ Motortech Z 2018;79(3):16–21. https://doi.org/10.1007/s35146-017-0184-y.
[6] Burger J, Ströfer E, Hasse H. Production process for diesel fuel components poly(oxymethylene) dimethyl ethers from methane-based products by hierarchical optimization with varying model depth. Chemical Engineering Research and Design 2013;91(12):2648–62. https://doi.org/10.1016/j.cherd.2013.05.023.
[7] Lumpp B, Rothe D, Pastötter C, Lämmermann R, Jacob E. Oxymethylene ethers as diesel fuel additives of the future. MTZ Worldw 2011;72(3):34–8. https://doi.org/10.1365/s38313-011-0027-z.
[8] Zhang X, Kumar A, Arnold U, Sauer J. Biomass-derived Oxymethylene Ethers as Diesel Additives: A Thermodynamic Analysis. Energy Procedia 2014;61:1921–4. https://doi.org/10.1016/j.egypro.2014.12.242.
[9] Breitkreuz CF, Schmitz N, Ströfer E, Burger J, Hasse H. Design of a Production Process for Poly(oxymethylene) Dimethyl Ethers from Dimethyl Ether and Trioxane. Chemie Ingenieur Technik 2018;72(3):34. https://doi.org/10.1002/cite.201800038.
[10] Schmitz N, Ströfer E, Burger J, Hasse H. Conceptual Design of a Novel Process for the Production of Poly(oxymethylene) Dimethyl Ethers from Formaldehyde and Methanol. Ind. Eng. Chem. Res. 2017;56(40):11519–30. https://doi.org/10.1021/acs.iecr.7b02314.
[11] Voggenreiter J, Burger J. Side Products in the Water-Tolerant Synthesis of Poly(oxymethylene) Dimethyl Ethers: Formation Kinetics and Implications for Process Design. Ind. Eng. Chem. Res. 2021;60(6):2418–29. https://doi.org/10.1021/acs.iecr.0c05780.
[12] Peláez R, Marín P, Ordóñez S. Synthesis of poly(oxymethylene) dimethyl ethers from methylal and trioxane over acidic ion exchange resins: A kinetic study. Chemical Engineering Journal 2020;396:125305. https://doi.org/10.1016/j.cej.2020.125305.
[13] Lautenschütz L, Oestreich D, Haltenort P, Arnold U, Dinjus E, Sauer J. Efficient synthesis of oxymethylene dimethyl ethers (OME) from dimethoxymethane and trioxane over zeolites. Fuel Processing Technology 2017;165:27–33. https://doi.org/10.1016/j.fuproc.2017.05.005.
[14] Wang D, Zhao F, Zhu G, Xia C. Production of eco-friendly poly(oxymethylene) dimethyl ethers catalyzed by acidic ionic liquid: A kinetic investigation. Chemical Engineering Journal 2017;334:2616–24. https://doi.org/10.1016/j.cej.2017.11.181.

[15] Wu Q, Wang M, Hao Y, Li H, Zhao Y, Jiao Q. Synthesis of Polyoxymethylene Dimethyl Ethers Catalyzed by Brønsted Acid Ionic Liquids with Alkanesulfonic Acid Groups. Ind. Eng. Chem. Res. 2014;53(42):16254–60. https://doi.org/10.1021/ie502409t.
[16] Burger J, Siegert M, Ströfer E, Hasse H. Poly(oxymethylene) dimethyl ethers as components of tailored diesel fuel: Properties, synthesis and purification concepts. Fuel 2010;89(11):3315–9. https://doi.org/10.1016/j.fuel.2010.05.014.
[17] Baranowski CJ, Bahmanpour AM, Kröcher O. Catalytic synthesis of polyoxymethylene dimethyl ethers (OME): A review. Applied Catalysis B: Environmental 2017;217:407–20. https://doi.org/10.1016/j.apcatb.2017.06.007.
[18] Bhatelia T, Lee WJ, Samanta C, Patel J, Bordoloi A. Processes for the production of oxymethylene ethers: promising synthetic diesel additives. Asia-Pac. J. Chem. Eng. 2017;12(5):827–37. https://doi.org/10.1002/apj.2119.
[19] Liu H, Wang Z, Li Y, Zheng Y, He T, Wang J. Recent progress in the application in compression ignition engines and the synthesis technologies of polyoxymethylene dimethyl ethers. Applied Energy 2019;233-234:599–611. https://doi.org/10.1016/j.apenergy.2018.10.064.
[20] Sonthalia A, Kumar N. Hydroprocessed vegetable oil as a fuel for transportation sector: A review. Journal of the Energy Institute 2019;92(1):1–17. https://doi.org/10.1016/j.joei.2017.10.008.
[21] Simacek P, Soucek I, Pospisil M, Vrtiska D, Kittel H. Impact of hydrotreated vegetable oil and biodiesel on properties in blends with mineral diesel fuel. Therm sci 2019;23(Suppl. 5):1769–77. https://doi.org/10.2298/TSCI180228315S.
[22] Vonortas A, Papayannakos N. Comparative analysis of biodiesel versus green diesel. WIREs Energy Environ 2014;3(1):3–23. https://doi.org/10.1002/wene.78.
[23] Al-Sabawi M, Chen J. Hydroprocessing of Biomass-Derived Oils and Their Blends with Petroleum Feedstocks: A Review. Energy Fuels 2012;26(9):5373–99. https://doi.org/10.1021/ef3006405.
[24] Pastor JV, García-Oliver JM, Micó C, García-Carrero AA, Gómez A. Experimental Study of the Effect of Hydrotreated Vegetable Oil and Oxymethylene Ethers on Main Spray and Combustion Characteristics under Engine Combustion Network Spray A Conditions. Applied Sciences 2020;10(16):5460. https://doi.org/10.3390/app10165460.
[25] No S-Y. Application of hydrotreated vegetable oil from triglyceride based biomass to CI engines – A review. Fuel 2014;115:88–96. https://doi.org/10.1016/j.fuel.2013.07.001.
[26] Hackbarth K, Haltenort P, Arnold U, Sauer J. Recent Progress in the Production, Application and Evaluation of Oxymethylene Ethers. Chemie Ingenieur Technik 2018;90(10):1520–8. https://doi.org/10.1002/cite.201800068.
[27] Preuß J, Munch K, Denbratt I. Performance and emissions of renewable blends with OME3-5 and HVO in heavy duty and light duty compression ignition engines. Fuel 2021;303:121275. https://doi.org/10.1016/j.fuel.2021.121275.
[28] Omari A, Heuser B, Pischinger S, Rüdinger C. Potential of long-chain oxymethylene ether and oxymethylene ether-diesel blends for ultra-low emission engines. Applied Energy 2019;239:1242–9. https://doi.org/10.1016/j.apenergy.2019.02.035.
[29] Jacob E, Bogatykh I, Goral T, Seidenspinner P, Wilharm T, Peter A et al. Synthetische Kraftstoffe gegen Klimawandel und für die Reinhaltung der Umwelt /Synthetic Fuels against Climate Change and Environmental Pollution. In: 41. Internationales Wiener Motorensymposium, II-114-II-148.

[30] Schmitz N, Friebel A, Harbou E von, Burger J, Hasse H. Liquid-liquid equilibrium in binary and ternary mixtures containing formaldehyde, water, methanol, methylal, and poly(oxymethylene) dimethyl ethers. Fluid Phase Equilibria 2016;425:127–35. https://doi.org/10.1016/j.fluid.2016.05.017.
[31] Mokbel I, Lindemann C, Duchet-Suchaux P, Jose J. Liquid–liquid equilibria of binary and ternary systems involving monoethyleneglycol, water, n-alkanes at three temperatures: 283.15, 303.15 and 333.15 K. Fuel 2016;163:17–24. https://doi.org/10.1016/j.fuel.2015.09.037.
[32] Sutton C, Calder JA. Solubility of higher-molecular-weight normal-paraffins in distilled water and sea water. Environ. Sci. Technol. 1974;8(7):654–7. https://doi.org/10.1021/es60092a007.
[33] Zhuang Z, Zhang J, Liu D. Liquid-liquid equilibria for ternary systems polyoxymethylene dimethyl ethers + water + n-hexane. CIESC Journal 2016;67(9):3545–51. https://doi.org/10.11949/j.issn.0438-1157.20160391.
[34] Shi M, Yu X, He G, Li Q. Liquid-liquid equilibrium for the ternary systems water + DMM 3 + (p -xylene, toluene, and n -heptane) at different temperatures. Can. J. Chem. Eng. 2018;96(4):968–77. https://doi.org/10.1002/cjce.23001.
[35] Shi M, He G, Gan F, Yu X, Li Q. Extraction of Low Concentration Aqueous Solution of Methylal: Liquid–Liquid Equilibrium in Water + Methylal + (Cyclohexane and n -Heptane) Ternary Systems. J. Chem. Eng. Data 2017;62(7):2183–90. https://doi.org/10.1021/acs.jced.7b00312.
[36] Li X, Tian H, Liu D. Liquid–Liquid Equilibrium for Ternary Systems of Polyoxymethylene Dimethyl Ethers + o -Xylene + Water at 293.15 K. J. Chem. Eng. Data 2019. https://doi.org/10.1021/acs.jced.8b00891.
[37] Li X, Cao J, Nawaz MA, Hu Y, Liu D. Experimental and Correlated Liquid–Liquid Equilibrium Data for Ternary Systems (Water + Poly(oxymethylene) Dimethyl Ethers + Toluene) at T = 293.15 and 303.15 K and p = 101.3 kPa. J. Chem. Eng. Data 2019;64(12):5548–57. https://doi.org/10.1021/acs.jced.9b00653.
[38] Gross J, Sadowski G. Application of the Perturbed-Chain SAFT Equation of State to Associating Systems. Ind. Eng. Chem. Res. 2002;41(22):5510–5. https://doi.org/10.1021/ie010954d.
[39] Gross J, Vrabec J. An equation-of-state contribution for polar components: Dipolar molecules. AIChE J. 2006;52(3):1194–204. https://doi.org/10.1002/aic.10683.
[40] Skjold-Jorgensen S, Kolbe B, Gmehling J, Rasmussen P. Vapor-Liquid Equilibria by UNIFAC Group Contribution. Revision and Extension. Ind. Eng. Chem. Proc. Des. Dev. 1979;18(4):714–22. https://doi.org/10.1021/i260072a024.
[41] Yang Z, Ren C, Jiang S, Xin Y, Hu Y, Liu Z. Theoretical predictions of compatibility of polyoxymethylene dimethyl ethers with diesel fuels and diesel additives. Fuel 2022;307:121797. https://doi.org/10.1016/j.fuel.2021.121797.
[42] Klamt A. Conductor-like Screening Model for Real Solvents: A New Approach to the Quantitative Calculation of Solvation Phenomena. J. Phys. Chem. 1995;99(7):2224–35. https://doi.org/10.1021/j100007a062.
[43] Yu M, Chen C, Jiang X. Understanding the miscibility of polyoxymethylene dimethyl ethers (OMEn) and diesel blend using molecular dynamics simulation. Fuel 2022;323:124348. https://doi.org/10.1016/j.fuel.2022.124348.

[44] Breitkreuz CF, Hevert N, Schmitz N, Burger J, Hasse H. Synthesis of Methylal and Poly(oxymethylene) Dimethyl Ethers from Dimethyl Ether and Trioxane. Ind. Eng. Chem. Res. 2022;61(23):7810–22. https://doi.org/10.1021/acs.iecr.2c00790.
[45] Schmitz N, Breitkreuz CF, Ströfer E, Burger J, Hasse H. Vapor-liquid equilibrium and distillation of mixtures containing formaldehyde and poly(oxymethylene) dimethyl ethers. Chemical Engineering and Processing: Process Intensification 2018;131:116–24. https://doi.org/10.1016/j.cep.2018.06.012.
[46] Wittig R, Lohmann J, Gmehling J. Vapor−Liquid Equilibria by UNIFAC Group Contribution. 6. Revision and Extension. Ind. Eng. Chem. Res. 2003;42(1):183–8. https://doi.org/10.1021/ie020506l.
[47] Gmehling J, Rasmussen P, Fredenslund A. Vapor-liquid equilibriums by UNIFAC group contribution. Revision and extension. 2. Ind. Eng. Chem. Proc. Des. Dev. 1982;21(1):118–27. https://doi.org/10.1021/i200016a021.
[48] Ohanamah MO, Thompson DW. Computation of multicomponent phase equilibria—Part II. Liquid-liquid and solid-liquid equilibria. Computers & Chemical Engineering 1984;8(3-4):157–62. https://doi.org/10.1016/0098-1354(84)87002-7.